Journal of Theoretical and Applied Information Technology
10th August 2015. Vol.78. No.1

ISSN: 1992-8645 www.jatit.org E-ISSN: 1817-3195

AUTOMATED BRAIN HEMORRHAGE LESION SEGMENTATION AND CLASSIFICATION FROM MR IMAGE USING AN INNOVATIVE COMPOSITE METHOD

[1]SUDIPTA ROY, [2]SANJAY NAG, [3]SAMIR KUMAR BANDYOPADHYAY,

[4]DEBNATH BHATTACHARYYA, [5]TAI-HOON KIM

[1, 2,3] Department of Computer Science and Engineering, [4]Department of Computer Application,

[5]Department of Convergence Security

[1]Academy of Technology, Adisaptagram, Hooghly-712121, West Bengal, India

[2,3] Calcutta University Technology Campus, JD-2, Sector-III, Salt Lake, Kolkata-98, India

[4]Vignan's Institute of Information Technology, Visakhapatnam-530049, AP, India

[5]Sungshin Women's University, 249-1, Dongseon-dong 3-ga, Seoul, 136-742, Korea

E-mail: [1]sudiptaroy01@yahoo.com, [2]sanjaynag75@gmail.com, [3]skb1@vsnl.com, [4]debnathb@gmail.com,

[5]taihoonn@daum.net

ABSTRACT

Accurate identification of acute hemorrhage is a critical step in planning appropriate therapy. The correct characterization of underlying pathology, such as neoplasia, vascular malformation, or infarction, is equally important for conclusive diagnosis. Computer-aided diagnosis (CAD) systems have been the focus of several research endeavors and it is solely based on the idea of analyzing images of different types of brain hemorrhage by implementing improved image processing algorithms. In this paper, an innovative and automated approach is cited to detect existence of brain hemorrhage in multiple MRI scan images of the brain, the type of hemorrhage and position of the hemorrhage. The implemented algorithm includes several stages such as artifact and skull elimination constituting preprocessing, image segmentation, and hemorrhage localization. The result of the conducted experiments has been compared statistically with reference image showing very promising results.

Keywords: *Brain, Hemorrhage, MRI, CAD, Hemorrhage Lesion, Image Segmentation, Position of Hemorrhage, Classification*

1. INTRODUCTION

In contemporary times, cerebrovascular diseases are the third cause of death in the world after cancer and heart diseases [1]. A common cerebrovascular diseases is brain hemorrhage which is caused by busting of one or more blood vessels within brain causing bleeding. There are many types of brain hemorrhage such as: epidural, subdural, subarachnoid, cerebral, and intra-parenchymal hemorrhage. The different types stated differ in many aspects such as the size of the hemorrhage region, its shape, and its location. MRI and CT are equally helpful for determining when hemorrhage is present [2]. MRI is more sensitive than CT for differentiating other types of neurological disorders that mimic the characteristics of stroke. MRI has a significant range of available soft tissue contrast, depicts anatomy in far greater details while at the same time being more sensitive and specific to abnormalities within the brain. Medical image segmentation attempts to label pixels by tissue type. Image segmentation play a significant role in many medical applications ranging from the education, assessment of medical students to image-guided surgery and surgical simulation. Appropriate segmentation methods have high correlation with image acquisition modality, the tissue of interest and since MRI provides superior contrast of soft tissue structures it is the choice of method for imaging the brain. Most research work on brain segmentation focuses on MRI for the same reason. The detection of hemorrhage is essential in the diagnosis and management of a variety of intracranial diseases including hypertensive hemorrhage, hemorrhagic infarction, brain tumor,

ISSN: 1992-8645 www.jatit.org E-ISSN: 1817-3195

cerebral aneurysm, vascular malformation, trauma, hemorrhagic changes following radio- or chemotherapy, and hemorrhagic pial metastasis. A recent report has indicated that the detection of hemorrhage on MR images is useful for the grading of gliomas. It has been found that T2-weighted gradient-recalled echo sequence is more sensitive than the T2-weighted spin-echo and fast SE sequences. The eason for this is the magnetic susceptibility induced by static field in-homogeneities arising from paramagnetic blood breakdown products. CAD systems incorporate computers to add a new dimension to physicians for achieving a faster and more accurate diagnosis. CAD systems are usually domain-specific as they are optimized for certain types of diseases, focuses on specific parts of the body and diverse diagnosis methods. They analyze different kinds of input such as stated symptoms, laboratory tests results, medical images, etc. corresponding to their specific domain. Diagnoses involving medical image interpretation systems are very useful since they can be integrated with the associated firmware and software accompanying the medical imaging machine to provide efficient and accurate diagnosis. Development of such CAD system is challenging since they combine the elements of artificial intelligence and digital images processing. This work proposes a CAD system to assist the radiologist for the detection of hemorrhages in MRI scan images of human brain and identify their types. Some of the older works [3, 4] addressed the problem of segmenting the region of intracerebral hemorrhages. The former work used a spatially weighted k-means histogram-based clustering algorithm, whereas in the latter work, the authors applied a multi resolution simulated annealing method. Cheng and Cheng [5] proposed a Fuzzy C-Means (FCM) method based on multi resolution pyramid for brain hemorrhage analysis. They also compared FCM, competitive Hopfield neural network [6] and fuzzy Hopfield neural network [7] in the global thresholding stage. In another work, Liu et al. [8] proposed an alternative fuzzy C-means method for the segmentation phase. A more contemporary work based on FCM is the work of Li et al. [9], used a thresholding technique based on FCM clustering to remove all non-brain regions. The results of this clustering were brain regions that were segmented into slices using median filtering to eliminate noise in the image, and then the maximum entropy threshold was computed for each slice to determine the potential hemorrhage regions. Region growing is not often used alone because it is not sufficient to segment brain structures accurately and robustly. The segmentation of light abnormality within the high background intensity performs unsatisfactorily result. It is observed that segmentation of dark abnormalities is not as effective as segmentation in light abnormalities. [10] Generalized fuzzy c-means algorithm uses both pixel attributes and spatial local information that is weighted in correspondence with neighbor elements based on their distance attributes. This has the potentiality to improve the segmentation performance tremendously. This improves the segmentation performance dramatically. Poor contrast, noise and non-uniform intensity variation can affect the results. The important phases of [11] paper are feature extraction, reduction of dimensionality, unsupervised data clustering, voxel classification and interactive post processing refinement. A result of the unsupervised 3D segmentation seems to be highly stable but a comparison with standard unsupervised methods (k-means) is not very significant in the clinical environment as a consequence of the segmentation of multivariate medical images. The color converted segmentation with Kmeans clustering algorithm and regions of the brain related to hemorrhage can be correctly separated from colored image and it help pathologist to distinguish lesion size and its region exactly. A first detection process [12] is based on selecting asymmetric areas with respect to the approximate brain symmetry plane. Its application to several datasets with different abnormality sizes, intensities and locations shows that it can automatically detect and segment very different types of brain abnormality with a good quality. A symmetric based [13] result constitutes the initialization of a segmentation method based on a combination of a deformable model and spatial relations, leading to a precise segmentation of the abnormalities. In the last phase of their work, the hemorrhage regions were determined according to their locations and gray level statistics. The result obtained is extremely encouraging; however, the authors acknowledged that it is a premature work. An enhancement process is applied for improving the quality of images along with mathematical morphology to increase the contrast in MRI images. Wavelet transform is applied in segmentation process for decomposition of MRI images [14]. The algorithms proposed in this research can contribute towards education of senior medical students/ resident doctors/ radiology students and further research in this field. The practical utility however is that it can assist in detecting hemorrhage through large sets of MRI of brain scans within very small time period.

ISSN: 1992-8645 www.jatit.org E-ISSN: 1817-3195

This paper is organized as follows: In this section a brief overview of related works was discussed. The proposed methodology is discussed in section 2. In section 3, the experimental results are portrayed to assess the quality of the proposed method on test dataset. In section 4, performance evaluation and accuracy measurement with ground truth image has been presented and finally we conclude our paper in section 5.

2. PROPOSED METHODOLOGY

The data set of "Whole Brain Atlas" image data base [15] which consists of T1 weighted, T2 weighted, proton density (PD) MRI image containing multiple image slice has been used. The RGB image has been converted to grayscale image using a weighted sum of the R, G, and B components multiplied by a constant. The transformation function is given below

$$g(x,y) = T[f(x,y)] \quad (1)$$

Here f(x, y) is the input image, g(x, y) is the processed image, and T is an operator on f, defined over some neighborhood of f(x, y). In addition, T can operate on a set of input images. The simplest form of T is when the neighborhood is of size 1×1 (that is, a single pixel). In this case, g depends only on the value of f at (x, y), and T becomes a gray-level (also called an intensity or mapping) transformation function of the form

$$s = T(r) \quad (2)$$

For maintaining simplicity in notation, r and s are variables denoting, respectively, the gray level of f(x, y) and g(x, y) at any point (x, y). This conversion is followed by image binarization, constituting the preprocessing step and threshold intensity is calculated by standard deviation of the image pixel intensity. To calculate the standard deviation, mean and variance derivation is written below. Mean is defined as the division of the number of samples multiplied by the sum of all data points

$$\mu = \frac{1}{MN}\sum_{x=0}^{M-1}\sum_{y=0}^{N-1} f(x,y) \quad (3)$$

Variance, is denoted as v, equals 1 divided by the number of samples minus one, multiplied by the sum of each data point subtracted by the mean then squared.

$$v = \frac{1}{MN}\sum_{x=0}^{M-1}\sum_{y=0}^{N-1}(f(x,y)-\mu)^2 \quad (4)$$

Standard deviation, denoted as σ, equals the square root of the variance s-squared is written below

$$\sigma = \sqrt{v} \quad (5)$$

The obtained standard deviation intensity value is used as threshold intensity to binarize the MR Image of brain and is very much helpful for extracting brain portion and differentiating it from to the non-brain portion. MRI of brain has the significant intensity difference between background and the foreground so the use of standard deviation based binarization has been successfully implemented for brain stroke detection purpose.

$$f1(x,y) = \begin{cases} 1 & \text{if } f(x,y) > \sigma \\ 0 & \text{if } f(x,y) \le \sigma \end{cases} \quad (6)$$

The negative of an image with gray levels in the range [0, L-1] is obtained by using the negative transformation is given by the expression

$$s = L - 1 - r \quad (7)$$

Reversing the intensity levels of an image in this manner produces the equivalent of a photographic negative and this type of processing is particularly suited for enhancing white or gray detail embedded in dark regions of an image, especially when the black areas are dominant in size. For binary image complement the algorithm use f2(x,y)=1-f1(x,y) which prepares it for the next step of wavelet decomposition. We begin by defining the wavelet series expansion of function f2(x) ϵ $L^2(R)$ relative to wavelet ψ(x) and scaling function φ(x). f2(x) can be represented by a scaling function expansion and some number of wavelet function expansions in sub-spaces W_{j_0} , W_{j_0+1}, W_{j_0+2} ….. Thus

$$f2(x) = \sum_k c_{j_0}(k)\varphi_{j_0}(x) + \sum_{j=j_0}^{\infty}\sum_k d_j(k)\psi_{j,k}(x) \quad (8)$$

Where j_0 is an arbitrary starting scale and the $c_{j_0}(k)$ and $d_j(k)$ are relabeled. The $c_{j_0}(k)$ normally called approximation or/and scaling coefficients; the $d_j(k)$ are referred to as detail or/and wavelet coefficients. Thus in the above equation first sum uses scaling function to provides an approximation of f2(x) at scale j_0. For each higher scale $j \ge j_0$ in the second sum, a finer resolution function a sum of wavelet is added to the approximation to provide increasing details. If the expansion function forms an

ISSN: 1992-8645 www.jatit.org E-ISSN: 1817-3195

orthogonal basis or tight frame, which is often the case, the expansion coefficients are calculated and is shown by the equations below

$$c_{j_0}(k) = < f2(x), \varphi_{j_0}(x) > = \int f2(x)\, \varphi_{j_0}(x)\, dx$$

and

$$d_j(k) = < f2(x), \psi_{j,k}(x) > = \int f2(x)\, \psi_{j,k}(x) dx \quad (9)$$

Above two coefficients expansion are defined as inner products of function being expanded and the expansion functions being used where φ_{j_0} and $\psi_{j,k}$ are the expansion functions; c_{j_0} and d_j are the expansion coefficients. Two dimensional (2-D) scaling function, $\varphi(x,y)$, which is a product of two 1-D functions and three two dimensional wavelets, $\psi^H(x,y)$, $\psi^V(x,y)$, and $\psi^D(x,y)$ are required. Excluding the products that produce 1-D results, like $\varphi(x)\,\psi(x)$, the four remaining products produce the separable scaling function and separable directionally sensitive wavelets

$$\varphi(x,y) = \varphi(x)\varphi(y)$$
$$\psi^H(x,y) = \psi(x)\psi(y)$$
$$\psi^V(x,y) = \psi(x)\psi(y)$$
$$\psi^D(x,y) = \psi(x)\psi(y) \quad (10)$$

The wavelets measure functional variations, intensity variations for images along different directions: ψ^H measures variations along columns, ψ^V measures variations along rows and ψ^D measures variations along diagonals. The directional sensitivity is a natural consequence of separability in the above equation and it does not increase the computational complexity. The method first defines the scaled and translated basis functions:

$$\varphi_{j,m,n}(x,y) = 2^{\frac{j}{2}}\, \varphi(2^j x - m, 2^j y - n)$$
$$\psi^i{}_{j,m,n}(x,y) = 2^{\frac{j}{2}}\, \psi^i(2^j x - m, 2^j y - n),$$
$$i = \{H, V, D\} \quad (11)$$

Here index i identifies the directional wavelets. The discrete wavelet transform of image f2(x, y) of size M×N is then denoted by the following equations

$$W_\varphi(j_0, m, n) = \frac{1}{\sqrt{MN}} \sum_{x=0}^{M-1} \sum_{y=0}^{N-1} f2(x,y)\varphi_{j_0,m,n}(x,y)$$

$$W_{\psi^i}(j, m, n) = \frac{1}{\sqrt{MN}} \sum_{x=0}^{M-1} \sum_{y=0}^{N-1} f2(x,y)\psi^i{}_{j,m,n}(x,y),$$

$$i = \{H, V, D\} \quad (12)$$

As in the 1-D case, j_0 is an arbitrary starting scale and the $W_\varphi(j_0, m, n)$ coefficients define an approximation f2(x, y) at scale j_0. The $W_{\psi^i}(j, m, n)$ coefficients add horizontal, vertical, and diagonal details for scales $j \geq j_0$. normally $j_0=0$ and $N=M=2^J$ so that $j=0,1,2,\ldots,J-1$ and $m=n=0,1,2,\ldots,2^j-1$. Thus f2(x, y) is obtained via the inverse discrete transform as obtained by the equation

$$f2(x,y) = \frac{1}{\sqrt{MN}} \sum_m \sum_n W_\varphi(j_0, m, n)\varphi_{j_0,m,n}(x,y) + \frac{1}{\sqrt{MN}} \sum_{i=H,V,D} \sum_{j=j_0}^{\infty} \sum_m \sum_n W_{\psi^i}(j, m, n)\psi^i{}_{j,m,n}(x,y) \quad (13)$$

After applying wavelet decomposition upto level two non-brain regions are totally separated from brain in a discrete form which is not useful for the approach as there is a possibility that abnormality may get lost and to rectify this problem a quick hull algorithms as proposed in [16] is implemented. The convex hull of a set of points in the plane is the shape taken by a rubber band that is placed "around the points" and allowed to shrink to a state of equilibrium. We can represent a point in the plane by a pair (x,y) that stores the x and y Cartesian coordinates for that point. We can represent a line l as a triple (a,b,c), such that these values are the coefficients a, b, and c of the linear equation ax+by+c = 0 associated with l. Given the Cartesian coordinates (x1, y1) of q1 and (x2, y2) of q2, the equation of the line l through q1 and q2 is given by

$$\frac{x-x_1}{x_2-x_1} = \frac{y-y_1}{y_2-y_1} \quad (14)$$

From this $a = (y_2-y_1)$; $b = -(x_2-x_1)$; $c = y_1(x_2- x_1) - x_1(y_2 -y_1)$ is derived. A line segment s1 is typically represented by the pair (p,q) of points in the plane that form s1's end points. It is possible to represent a polygon P by a circular sequence of points, called the vertices of P. The segments between consecutive vertices of P are called the edges of P. Polygon P is said to be nonintersecting, or simply, if intersections between pairs of edges of P happen only at a common endpoint vertex. A polygon is convex if it is simple and all its internal angles are less than p. Quick-hull described in [16] is a divide-and-conquer algorithm, similar to quick sort, which divides the problem into two sub-problems and discards some of the points in the given set as

ISSN: 1992-8645 www.jatit.org E-ISSN: 1817-3195

interior points, concentrating on remaining points. Quick-hull runs faster than the randomized algorithms because it processes fewer interior points. Also, Quick-hull reuses the memory occupied by old facets. The convex image is now a binary image in which only brain portion is denoted with one and all non-brain portion contains zero. This convex image is multiplied with original image and the resultant image is devoid of any previously existing artefact, noise and skull as such removal is critical for brain abnormality detection. Then the power-law transformations is applied which has the basic form of

$$f4(x,y) = c * f3(x,y)^{\gamma} \quad (15)$$

Where c and γ are the positive constant and the above equation is sometimes written as

$$f4(x,y) = c * (f3(x,y) + \varepsilon)^{\gamma} \quad (16)$$

To report for a measurable output when the input is zero we use ε. However, offsets typically are an issue of display calibration and as a result they are generally ignored. Transform values of γ>1 have accurately the opposite effect as those generated with principle values of γ <1 and to the identity transformation when c= γ =1. Gamma correction is significant for displaying an image appropriately on a computer screen and particular care must be taken to reproduce colors accurately. This requires knowledge of gamma correction as any change in the value of gamma will not only alter the brightness but also the corresponding red, green and blue ratios. By using this gamma transformation the abnormal portion can be more prominently projected. The total intensity, by sum of the average and standard deviation of the gamma transformed image is finally selected. Thus the final selection is given by

$$T = \frac{1}{MN}\sum_{x=0}^{M-1}\sum_{y=0}^{N-1} f4(x,y) + \sqrt{\frac{1}{MN}\sum_{x=0}^{M-1}\sum_{y=0}^{N-1}(f4(x,y)-\mu)^2} \quad (17)$$

On the basis of the final intensity value we find the hemorrhage portion which in the form of binary output and is stored in f5(x, y). It is possible to classify different type of hemorrhage by multiplying the original input image or the image where skull has been excluded. We use first derivative to detect the contour of the detected brain hemorrhage. The first derivative denotes zero in areas of constant gray-level values while non-zero at the onset of a gray-level step or ramp; and must be nonzero along ramps. Since we are dealing with digital quantities whose values are finite, the maximum possible gray-level change is also finite, and the shortest distance of change can occur between adjacent pixels. A basic definition of the first-order derivative of a one-dimensional function f(x) is the difference. While dealing with binary image for the detection of the contour, the first derivative can be applied for the detection of the same. Horizontal contour is defined by

$$h_c = \frac{\partial f}{\partial x} = f5(x+1) - f5(x)$$

Vertical contour is defined by

$$v_c = \frac{\partial f}{\partial y} = f5(y+1) - f5(y) \quad (18)$$

Horizontal and vertical contour detection does not produce continuous line so for contour detection the horizontal and vertical contour is combined by

$$c_c = h_c + v_c \quad (19)$$

For abnormality location detection it is needed to calculate centroide of the brain stroke region by which it is possible to classify the type of hemorrhage. This is done by utilizing weighted mean of the pixels and mathematical deduction of centroid is given below:

$$X_{cood} = \sum_{n=1}^{p} x_n I_n / \sum_{n=1}^{p} I_n$$
$$Y_{cood} = \sum_{n=1}^{p} y_n I_n / \sum_{n=1}^{p} I_n \quad (20)$$

The abnormal regions from the top, bottom, left and right to the centroid of the brain is obtained using simple mathematical formulation utilizing only the distance between two points.

3. RESULTS AND DISCUSSION

The algorithm mentioned here has been tested to establish the superiority of the outcome generated by the proposed method using proper data set and appropriate mathematical formulation. For Classification of MRI hemorrhage lesion, it is possible to conceptually treat hemorrhage lesion as

Journal of Theoretical and Applied Information Technology
10th August 2015. Vol.78. No.1

ISSN: 1992-8645 www.jatit.org E-ISSN: 1817-3195

two ellipses and calculate semi major, semi minor axis with eccentricity and with respect to this value it can be categorized as chronic subdural hematoma. If ellipse formation is possible, then from the position its distance from the skull and area of lesion is calculated. With such calculation it can be classified as cerebral hemorrhage, vascular dementia, intra-parenchymal hemorrhage and acute stroke.

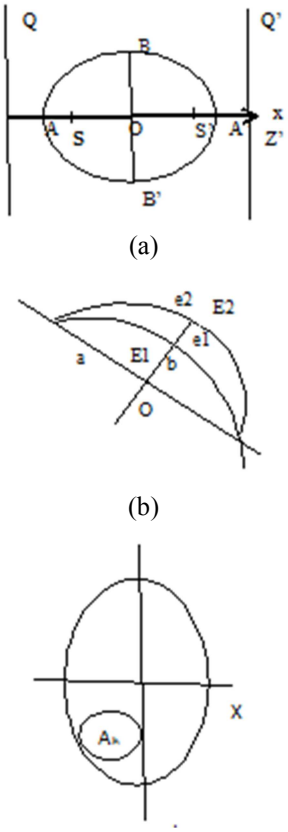

Figure. 1: Schematic diagram of hemorrhage classification: a) elliptic nature, b) edge of abnormality is consider as two different ellipse, c) position of abnormality (Ab)with inter and intra distance.

From the above Figure 1 (a) consider the foci S, S' are the points (-ae,0) , (ae,0), the directories ZQ, Z'Q' are lines x=-a/e, x=a/e, AA' is the major axis, BB' is the minor axis and O the centre of the ellipse. AA'=2a; BB'=2b; thus the eccentricity e of the ellipse is $b^2=a^2(1-e^2)$

From the equation

$$y^2 = b^2\left(1-\frac{x^2}{a^2}\right), |x| \le a \qquad (21)$$

The area of the ellipse is 4 times the area in the positive quadrant and area A is

$$A = 4\int_0^a y\,dx \qquad (22)$$

The area obtained after segmentation is then verified using area difference between two ellipses. The algorithm concentrates on the position of lesion, skull distance and center distance. The epidural hemorrhage is characterized by its convex shape and its close fitting with the skull. The subdural hemorrhage is similar to the epidural one regarding its closeness to the skull; however, the size of subdural hemorrhage is larger than that of the epidural one and it has a crescent-like shape with a concave surface away from the skull. Finally, the intra-parenchymal hemorrhage is characterized by its distance from the skull. The appearance and evaluation of intracranial hemorrhage shown on MRI primarily depend on the age of hematoma and on the imaging sequence (T1 weighted, T2 weighted, PD). In the figure 2 shown below, hemorrhage has been found on the left lobe of the brain. There is no relation with the skull portion and it is classified as cerebral and intracranial hemorrhage. In the experiments conducted, the algorithm is implemented on T2, T1, PD type of MRI images for cerebral hemorrhage detection and the methods successfully detected abnormality but when applying to other kind of hemorrhage detection the skull elimination steps are excluded. The images shown belong to a 49-year-old African-American woman [15] with a history of hypertension and diabetes mellitus. The scan was performed when the patient experienced numbness and tingling of the left leg for about one day. Systemic arterial blood pressure was 240/130. There was no weakness, facial droop, visual change; no upper extremity or right lower extremity sensory abnormality; no bowel or bladder dysfunction; no headache, fever, shortness of breath, chest pain, nausea, vomiting, diaphoresis, vertigo or light-headedness, no back pain, and no history of seizures. Epidural hematoma is located into the potential space between the dura, which is inseparable from cranial periosteum, and the adjacent bone. Subdural hematoma is diagnosed on the basis of mass effect, which is depicted as displacement of the blood vessels on angiograms on skull. Subarachnoid hemorrhage appears when bleeding happens into the subarachnoid space around the brain and spinal cord. The testing dataset [15] consists of 60 MRI images of human brain with different type of hemorrhage including some normal brain image. Among the images 20 set is of normal brain while the remaining images represent brains with at least one of the three types of brain hemorrhage. An image of a normal brain shows a distribution of gray matter that appears clear in the texture-like fissures, while an abnormal

ISSN: 1992-8645 www.jatit.org E-ISSN: 1817-3195

brain has a shape which appears brighter than the normal gray matter. Generally, abnormal regions of the brain differ in characteristics than the normal brain but the diversity of characteristics is notable when compared to any other organ for T1, T2, PD type of MRI images. Thus accurate segmentation is very important and considerable attention has been given to achieve the same. For brain hemorrhage segmentation several steps has been proposed and details are shown in Figure 2 below. The Figure 2(A) is the input MRI of brain and Figure 2(B) is the complemented form of the binary image and wavelet decomposition up to level two has been applied to extract the brain from any artifact and other non-brain portion. Then the image is complemented with the wavelet decomposed image followed by application of quick-hull algorithms for convex hull to produce continuous object image which is shown in Figure 2(C). Figure 2(D) is the output image after power law transformation has been applied on the convexed image which is helpful to segment the brain hemorrhages using expectation maxima. Figure 2 (E) shows binary segmented hemorrhage portion. In Figure 2(F) depicts the hemorrhage portion within the brain image marked by red region for visualization. Figure 2(G) shows the contour detection by horizontal contour detection and Figure 2(H) show the vertical contour detection. Contour lines are not continuous for the horizontal and vertical contour that is why both are combined to obtain the final contour image which is continuous and is shown in Figure 2(I). Figure 2(J) shows the localization of hemorrhage and accordingly classified based on their localization information into different types of brain hemorrhage.

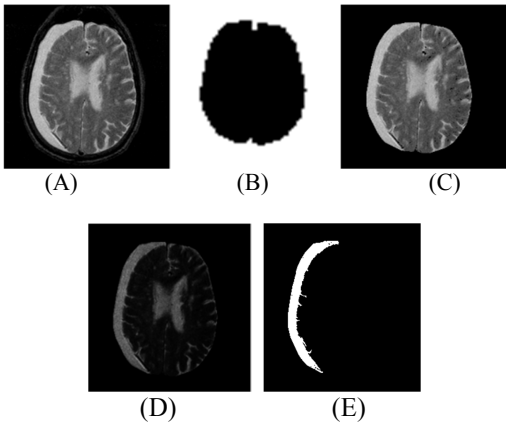

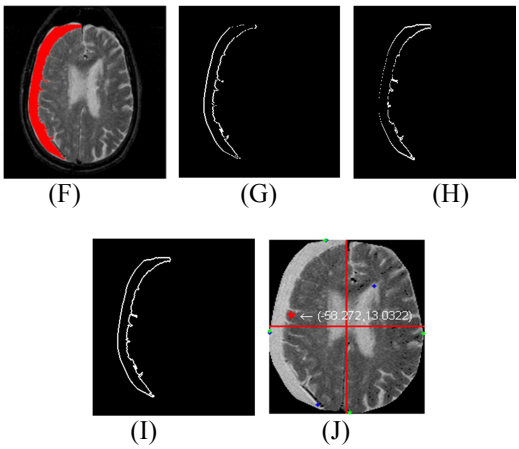

Figure 2 : A) Input MRI of Brain , B) complemented wavelet decomposed output, C) applying convex hull, D) after gamma transformation, E) segmented abnormal portion, F) abnormal portion indicated by red marks, G) horizontal contour, H) vertical contour, I) contour of abnormal region, J) localization of abnormal region.

We have tested another set of images from a 76 year old man [15], who suffered a severe fall 6 months before the scan. He sought medical attention only after he complained of memory loss. He was depressed since the death of his wife. The patient had a history of alcoholism with several hospital admittance of gastrointestinal bleeding. The large fluid collection displacing the brain can be observed. It is showing as a high intensity white zone on T2-weighted images and non-perfused on SPECT. The lateral and third ventricles are a bit large, partly due to the effects of age and partly to the effects of alcohol abuse. The mammillary bodies are small in this case compared to the normal, a finding commonly seen in alcoholics. Representation of the interior architecture and localization of hemorrhagic lesions is important because the appearance of the internal structure helps to understand the stage of hematomas or to differentiate idiopathic hemorrhage from hemorrhage caused by pathologic conditions, such as intra-axial tumor or vascular malformation. As already discussed, different type of hemorrhage case depends on the quantification and location of the abnormality portion has been presented in Table 1 with their location. Subdural hematoma occurs when there is a rupture of the bridging cortical veins and a hematoma not in direct contact with the brain surface is distinguished pathologically from subdural hematoma with adjacent contusion. Acutely, the T1-weighted image demonstrates the hematoma to have signal similar to normal cortex, and an underlying darker irregular band reflecting the acute contusion and edema which has prolonged bulk T1 relaxation. Prolonged T2 relaxation in both

Journal of Theoretical and Applied Information Technology
10th August 2015. Vol.78. No.1

ISSN: 1992-8645 www.jatit.org E-ISSN: 1817-3195

regions is reflected in the long TR/TE. These images demonstrate high signal regions usually separated by a narrow strip of very low signal and cerebral hemorrhage has the direct contact with the brain surface. The positions of different abnormality are shown in table 1 below coordinate wise.

Table 1: Position of abnormality for different kind of MRI

Image name	Center to Centroid		Top to Top	Bottom to Bottom	Left to Left	Right to Right
	X-Coordinate	Y-Coordinate				
11_PD	-34.4	3.78	72.20	65.45	23.25	83.60
12_PD	-33.8	-12.5	92.70	60.41	23.25	96.15
13_PD	-30.1	-5.09	58.69	46.04	39.29	85.40
14_PD	-26.6	-12.0	67.77	48.37	26.47	78.44
11_T1	-31.5	3.84	78.79	80.60	35.90	98.70
12_T1	-32.8	-6.44	91.78	72.18	32.31	96.13
13_T1	-31.5	-10.2	99.36	75.18	36.35	95.59
11_T2	-35.1	3.60	70.49	63.89	22.09	81.45
12_T2	-43.0	-15.2	100.8	59.13	16.00	100.9
13_T2	-33.0	-27.2	114.7	52.46	38.60	85.00
13_T2	-25.3	-17.7	80.36	50.04	45.8	80.41
30_T2	-59.4	15.60	4.00	22.13	1.000	72.85
31_T2	-58.2	13.03	1.000	35.17	2.000	76.49
32_T2	-55.4	7.74	1.000	2.236	2.000	54.51
33_T2	-54.9	8.14	1.000	7.21	3.162	128.1
38_T2	-48.7	5.50	6.082	13.89	21.00	125.0
40_T2	-43.2	8.31	3.162	5.099	8.000	98.35

The objective of this work is to correctly classify brain MRI images into one of five classes: normal, epidural hemorrhage (removing skull elimination step), subdural hemorrhage (removing skull elimination step), cerebral hemorrhage (including skull elimination step) and intra-parenchymal hemorrhage (including skull elimination step) by finding their location from Table 1 as well as visual inspection. The system has ability to distinguish between normal and abnormal cases which are also important for automated medical image analysis.

4. COMPARISON AND PERFORMANCE ANALYSIS

Accurate diagnosis of brain abnormality patients, proper segmentation method is required to be used for MR images to carry out an improved diagnosis and treatment. Currently, information is provided by many images from various slices required for diagnosis, planning and treatment purpose. The performance evaluation of image segmentation methods is a challenge for medical image analysis system. Accuracy is important for the segmentation technique of the proposed system as it confers to the degree to which the segmentation results agree with the ground truth. The accuracy measures used to evaluate the performance of the proposed methods are the Relative area Error (RE), Kappa Index (KI), Jacard Index (JI), and Correct Detection (CD). We compare our proposed method has been compared with K-means [12], symmetric based [13], FCM [10], and morphology [14] based method. The column chart graphical representation of the different performance evaluation metric RE, KI, and JI has been shown in Figure 3, Figure 4, and Figure 4 below.

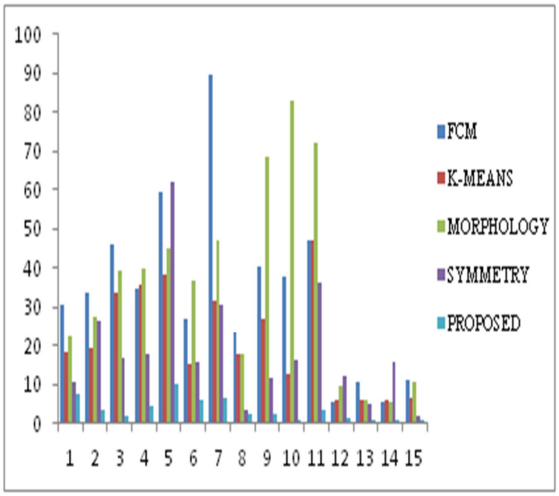

Figure 3: 2D column chart representation of the RE metric

A critical problem faced in performance evaluation of segmentation methods is the lack of a gold standard. Although physical or digital phantoms can provide "ground truth", they are still unable to reproduce the full range of imaging characteristics, normal and abnormal anatomical variability observed in clinical data. Kappa index is determined by the double of intersection of automated and manual segmentation divided by sum of automated and manual segmentation [16]. False positive can be determine automated subtracted by intersection and false negative can be determine manual subtracted by intersection. Jaccard index is determined by intersection of automated and manual segmentation divided by summation of intersection, false positive and false negative. Correct detection ratio is determined by intersection divided by manual segmentation. Relative area error is determined by difference

Journal of Theoretical and Applied Information Technology
10th August 2015. Vol.78. No.1

ISSN: 1992-8645 www.jatit.org E-ISSN: 1817-3195

between automated to manual divided by manual segmentation.

We represent the column chart from the table value and from the average of RE proposed method give the best results. Symmetry is second best, third best Kmeans, forth best morphology and then FCM based segmentation. (Average vales of FCM=33.4283, Kmeans=21.3019, Morphology=35.3310, Symmetry=18.7486, and proposed method=3.40523.)

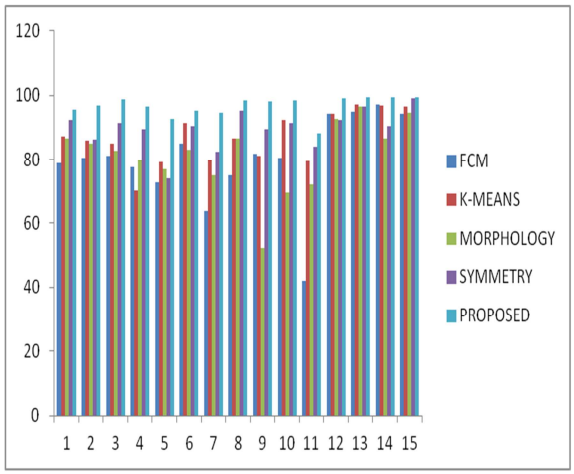

Figure 4: 2D column chart representation of the KI metric

From the average value of KI proposed method give the best results. Symmetry is second best, third best Kmeans, forth best morphology and then FCM based segmentation. (Average vales of FCM=79.9939, Kmeans=86.8896, Morphology=81.3111, Symmetry=89.5944, proposed method=96.6799.)

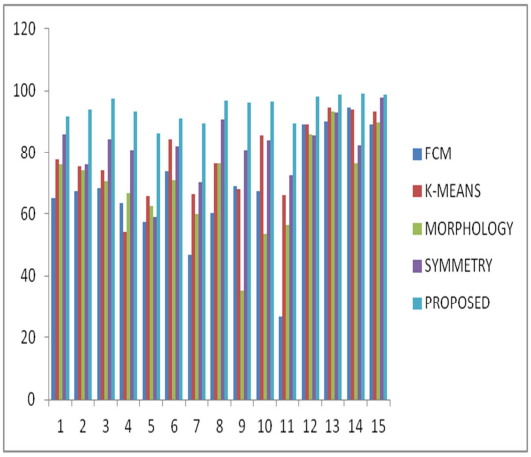

Figure 5: 2D column chart representation of the JI metric

From the average value of JI proposed method give the best results. Symmetry is second best, third best Kmeans, forth best morphology and then FCM based segmentation. (Average vales of FCM=68.5753, Kmeans=77.6129, Morphology=69.8183, Symmetry=81.6405, proposed method=94.4427.) The Kappa index is sensitive to both differences in size and location and differences in location are more strongly reflected than differences in size and K_i > 90% indicates a good agreement. The kappa index calculated on experimental results achieved by implementing the proposed methods reaches 96.6799%. Jacard index is more sensitive to differences since both denominator and numerator change with increasing or decreasing overlap and in the proposed methodology maximum times it gives greater than 90% (average value 94.4427%) which indicates that the experiment results are promising. The average value of RE in proposed method is 3.40523 which is very low value than other methods. We attempted to evaluate the performance of the worthwhile recent research works done on brain abnormality detection and segmentation. Through analysis of the literature, we found that automation of brain abnormality detection and segmentation from brain MR images is one of the most active research areas and enormous research has been done in this area for the last many years. However, the overlap measure depends on the size and the shape complexity of the object and is related to the image sampling. Maximum methods fail to produce proper output due to large intensity difference of MR images and some method depends on other intensity based preprocessing method which is not perfect. We overcome problem of segmentation and our methodology gives very superior results visually as well as quantifiably.

5. CONCLUSION

Accurate measurements of clot thickness, hematoma area, and localization of lesion from MRI scan have been successfully implemented by the proposed system. This is critical for early, reliable and accurate detection of hemorrhage for providing early diagnosis and treatment, prompt transfer of the patient to a medical facility capable of MRI scanning and neurological intervention if necessary. Automated systems for analyzing and classifying medical images have gained a great level of attention and the methods proposed will positively contribute to the betterment of such system. The results obtained are encouraging with

ISSN: 1992-8645 www.jatit.org E-ISSN: 1817-3195

higher accuracy for the 3-class classification problem. The system will provide even better results when implemented on a better dataset with high resolution images taken directly from the MRI of brain. The proposed methods have capabilities beyond brain hemorrhage detection and can be utilized for future system on other MR images. The proposed CAD can assist the radiologist for better detection and classification of Brain hemorrhage and hence can prove itself as an asset to any medical establishment dealing with brain hemorrhages. This is considered to be one of the most important but difficult part of the process of detecting brain abnormality. Hence, detecting brain abnormality and classification is highly successful that segmentation of the MRI images must be done accurately by computer to do the exact diagnosis.

ACKNOWLEDGEMENTS

It is my privilege to thank the Dr. Pradip Saha, is MD in Radiology from NRS Medical College and ex-Faculty from there. He is currently radiologist at M N Roy Diagnostic Center, Kolkata, India. He have supported for reference image creation, guided, and given us the valuable suggestions to complete this paper, and to enrich my knowledge.

REFERENCES

[1] Y. Li, Q. Hu, J. Wu, and Z. Chen "A hybrid approach to detection of brain hemorrhage candidates from clinical head ct scans," In Sixth International Conference on Fuzzy Systems and Knowledge Discovery (FSKD), pages 361–365, 2009.

[2] http://nihseniorhealth.gov/stroke/preventionanddiagnosis/01.html, (available at: May, 2013.)

[3] S. Loncaric, A. Dhawan, J. Broderick, and T. Brott, "3-d image analysis of intra-cerebral brain hemorrhage from digitized ct films," Computer Methods and Programs in Biomedicine, 46(3):207–216, 1995.

[4] S. Loncaric and Z. Majcenic, " Multiresolution simulated annealing for brain image analysis :In Medical Imaging," International Society for Optics and Photonics, pp. 1139–1146, 1999.

[5] D. Cheng and K. Cheng, "Multiresolution based fuzzy c-means clustering for brain hemorrhage analysis," In Proceedings of the 2nd International Conference on Bioelectromagnetism, pages 35– 36, IEEE, 1998.

[6] K. Cheng, J. Lin, and C. Mao, "The application of competitive hopfield neural network to medical image segmentation," IEEE Transactions on Medical Imaging, 15(4):560–567, 1996.

[7] J. Lin, K. Cheng, and C. Mao, "A fuzzy Hopfield neural network for medical image segmentation," IEEE Transactions on Nuclear Science, 43(4):2389–2398, 1996.

[8] H. Liu, C. Xie, Z. Chen, and Y. Lei, "Segmentation of ultrasound image based on morphological operation and fuzzy clustering," In Third IEEE International Workshop on Electronic Design, Test and Applications (DELTA), 2006.

[9] Y. Li, Q. Hu, J. Wu, and Z. Chen, "A hybrid approach to detection of brain hemorrhage candidates from clinical head ct scans," In Sixth International Conference on Fuzzy Systems and Knowledge Discovery (FSKD), pages 361–365, 2009.

[10] Van Lung, H., & Kim, J. M, "A generalized spatial fuzzy c-means algorithm for medical image segmentation," In Fuzzy systems, 2009. FUZZ - IEEE 2009. IEEE Internatinal Conference on (pp. 409-414).

[11] Schenone, A., Firenze, F., Acquarone, F., Gambaro, M., Masulli, F., & Andreucci, L. (1996), " Segmentation of multivariate medical images via unsupervised clustering with adaptive resolution," Computerized medical imaging and graphics, 20(3), 119-129.

[12] Juang, Li-Hong, and Ming-Ni Wu. "MRI brain lesion image detection based on color converted K-means clustering segmentation." Measurement 43.7 (2010): 941- 949.

[13] Hassan Khotanlou, Olivier Colliot and Isabelle Bloch, "Automatic brain tumor segmentation using symmetry analysis and deformable models" Ecole Nationale Superieure des Telecommunications, pp. 1-6

[14] Kharrat, A., Benamrane, N., Ben Messaoud, M., & Abid, M, "Detection of brain tumor in medical images," In Signals, Circuits and Systems (SCS), 2009 3rd International Conference on (pp. 1-6). IEEE

[15] http://www.med.harvard.edu/AANLiB/cases/, (available at: July, 2013)

[16] C. Bradford Barber, David P. Dobkin, Hannuhuhdanpaa, "The Quickhull Algorithm for Convex Hulls," ACM Transactions on Mathematical Software, Vol. 22, No. 4, December 1996, Pages 469–483.

ISSN: 1992-8645 www.jatit.org E-ISSN: 1817-3195

[17] S Roy, S K Bandyopadhyay, "A Review on Volume Calculation of Brain Abnormalities from MRI of Brain using CAD system," International Journal of Information and Communication Technology Research, Volume 4 No. 4, pp. 114-120, April 2014.

[18] S Roy, S Sadhu, S K Bandyopadhyay "A Useful Approach towards 3D Representation of Brain Abnormality from Its 2D MRI Slides with a Volumetric Exclamation," Proc. IEEE, C3IT, West Bengal, February 2015.

[19] S Roy, P Ghosh, S K Bandyopadhyay, "Segmentation and Contour Extraction of Cerebral Hemorrhage from MRI of Brain by Gamma Transformation Approach," FICTA-2014, Proc. Springer, AISC 328, Bhubaneswar, Orissa.

[20] S Roy, P Ghosh, S K Bandyopadhyay, "A Framework for Volumetric Computation of Brain Abnormality from MRI of Brain Slice and Its Appropriateness Measurement," ICC-2014, Bangalore, Proc. Elsevier, Digital Signal and Image Processing, Bangalore, pp. 29-36, 2014.

[21] S Roy, K Chatterjee, S K Bandyopadhyay, "Segmentation of Acute Brain Stroke from MRI of Brain Image Using Power Law Transformation with Accuracy Estimation," ICACNI-2014, Kolkata, Proc. Springer, Smart Innovation, Systems and Technologies, Volume 27, 2014, pp 453-461.

[22] S Roy, S K. Bandyopadhyay, "Abnormal Regions Detection and Quantification with Accuracy Estimation from MRI of Brain," 2013 2nd IMSNA, Canada, Proc. IEEE, pp. 611-615, 2013.

Journal of Theoretical and Applied Information Technology
10th August 2015. Vol.78. No.1

ISSN: 1992-8645 www.jatit.org E-ISSN: 1817-3195

Appendix: More Results

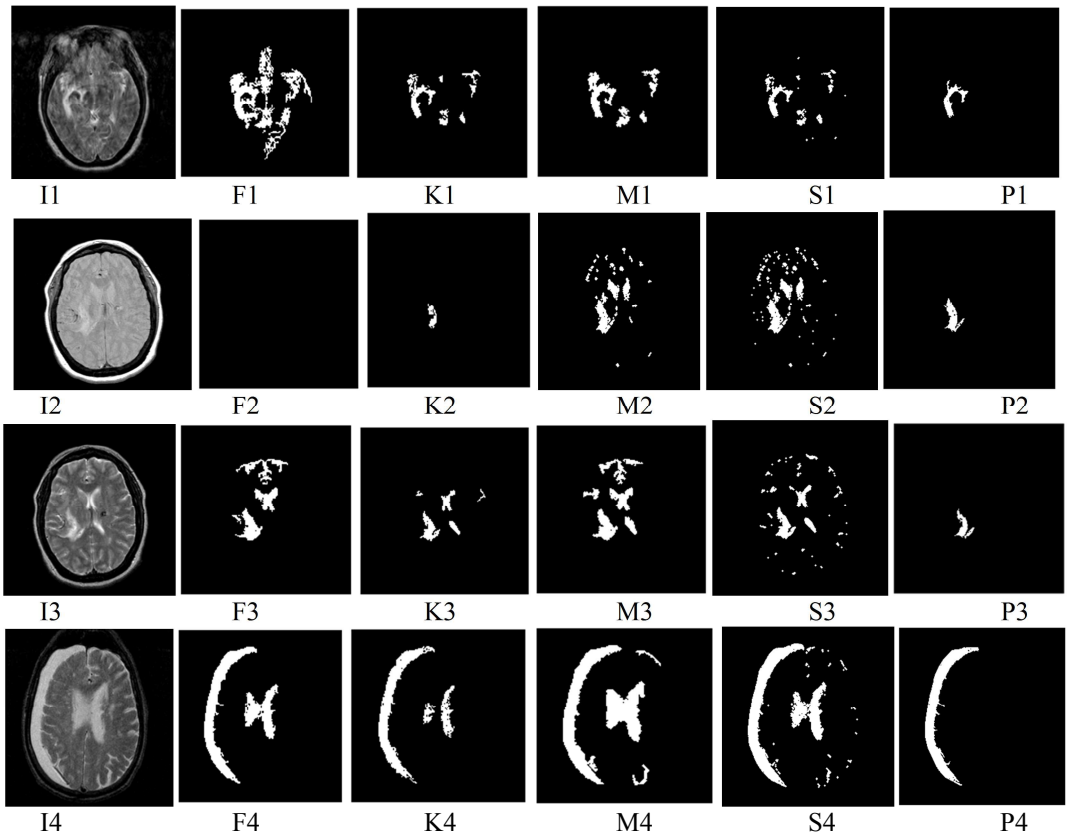

Figure 6: Different output for different input image; (I1, I2, I3, I4) are the input image, (F1,F2,F3,F4) are the output by FCM, (K1,K2,K3,K4) are the output by Kmeans, (M1,M2,M3,M4) are the output by Morphology , (S1,S2,S3,S4) are the output by Symmetry, (P1,P2,P3,P4) are the output by Proposed methods.